Co-influencing mechanisms of physicochemical properties of blasting dust in iron mines on its wettability

Jian-guo Liu[1,2,3], *Long-zhe Jin*[1,2,3], *Jia-ying Wang*[1,2,3], *Sheng-nan Ou*[1,2,3], *and Tian-yang Wang*[1,2,3]

1) School of Civil and Resource Engineering, University of Science and Technology Beijing, Beijing 100083, China

2) Key Laboratory of High-Efficient Mining and Safety of Metal Mines of the Ministry of Education, University of Science and Technology Beijing, Beijing 100083, China

3) Mine Emergency Technology Research Center, University of Science and Technology Beijing, Beijing 100083, China

Abstract: This study explores the key physicochemical factors affecting the hydrophilic characteristics of iron mine blasting dust (BD). The BD is separated into an unwetted part (UWBD, hydrophobic part) and a wetted part (WBD, hydrophilic part). Its particle size, true density (TD), pore parameters, mineral composition, and surface compounds are comprehensively characterized and compared. The results indicate that a smaller particle size and more developed pore parameters are two key factors responsible for the strong hydrophobicity of the BD. The mineral composition of the BD has no direct effect on its wetting properties; however, it indirectly influences the deposition characteristics of the BD in water by affecting its TD. Unlike coal dust, the surface organic composition of the BD does not affect its wettability and the peak area of C–C/C–H hydrophobic groups in the C 1s X-ray photoelectron spectrum of the UWBD (45.03%) is smaller than that in the C 1s spectrum of the WBD (68.30%). Thus, eleven co-influencing processes of physicochemical properties of the BD on its wettability are summarized. This research sheds light on the key factors affecting the wettability of the BD.

Keywords: blasting dust; physicochemical characteristics; hydrophilic; contact angle; iron mine

1. Introduction

Air pollution has become a global problem in the twenty-first century. However, blasting, which is accompanied by the massive emission of dust and toxic gases such as nitrogen oxides and carbon oxides, remains the main mining technology in metal mines worldwide [1−2]. In general, these substances containing large amounts of metals are exhausted directly into the atmosphere through ventilation after blasting in either opencast or underground mines. They can rapidly form aerosol particles in the atmosphere at a certain temperature and humidity and can diffuse with the wind over long distances [3]. In addition, these particulate matters become suspended in the underground air, which not only increases miners' risk of pneumoconiosis but also reduces visibility in the underground environment and increases the possibility of severe accidents. Therefore, blasting explicitly poses a unique risk to human health and the environment. The number of pneumoconiosis cases in China has increased from 9173 in 2005 to 26873 in 2015 [4]. Therefore, eliminating or at least controlling the emission of dust from mining operations, particularly from the processes of blasting and roadway driving, crushing, and grinding, is important.

Over the past few decades, extensive efforts have been devoted to reducing the emission of mining dust (MD) by investigating the generation mechanism [5−6], diffusion process [7−8], and toxicology [9] of MD. Some efficient MD control techniques, such as ventilation [7−8], water spray [10], foam technology [11], chemical dust suppressants [12−13], and surfactant-magnetized waters [14], have been proposed and applied in the field. These studies have demonstrated that the physical and chemical properties of dust not only pose risks to human health and the environment but also dominantly affect the wettability of dusts, which directly determines the suppression efficiency of water-based dust reduction techniques. Therefore, it is necessary to study the physicochemical properties of MD to ena-

🐾 Springer

ble the selection of an appropriate method for its control and to improve the suppression efficiency.

Generally, the physical properties of dust include its particle size distribution (PSD), micromorphology, porosity, specific surface area (SSA), and its density [15–19]. The hydrophobicity of coal dust increases with decreasing particle size, which has been attributed to the higher surface energy of finer particles, as demonstrated by Yang *et al.* [20]. However, Kollipara *et al.* [16] observed the opposite experimental result—that coarser particles require more time to be wetted—which might be a consequence of their atypical surface chemical properties. Moreover, pore parameters, including surface area, pore size, and pore volume, are other dominant physical factors affecting the wettability of MD [17,20], which are heavily affected by the coal rank [17,20–23]. The more developed and complicated the pore structures, the poorer the wettability of the dust because the stronger gas adsorption capacity can easily form a gas film around the coal dust, which weakens the wetting process [12]. In addition, the surface chemical properties of dust affect its wetting process. Xu *et al.* [23] investigated the influence of chemical properties of coal dust on its wettability in detail, demonstrating that coal dust with high hydroxyl and moisture contents has a fast wetting rate. Zhou *et al.* [24] suggested that the content of oxygen-containing polar group serves as a more reasonable indicator of the coal dust wettability. Moreover, Machado *et al.* [18] studied the physicochemical and morphological properties of the electric arc furnace dust because large quantities of elements Fe and Zn are contained in it. As mentioned above, although the influence of the physical and chemical properties of dust on its wettability has been studied separately in much detail, the co-influencing mechanisms of the physical and chemical properties of dust on its wetting process are seldom investigated.

The blasting dust (BD) of iron mines contains a substan-

tial amount of Fe and Si that become highly hazardous to the environment and to human health when discharged directly into the atmosphere. Therefore, effective dust suppression measures are needed after blasting in an iron mine. The suppression efficiency is known to be critically affected by the wettability of dust, which is determined by the physicochemical properties of dust, as previously mentioned. However, only a few articles about the physicochemical properties of the BD and their co-influencing actions on its wettability are currently available.

In this study, first, the BD samples are separated into two parts using deionized water: the unwetted part (unwetted blasting dust [UWBD], hydrophobic part) and the wetted part (wetted blasting dust [WBD], hydrophilic part). Next, the physical and chemical properties of the UWBD and WBD parts are comprehensively characterized and compared with each other. Lastly, the key influencing factors and their co-affecting mechanisms on the BD wettability are proposed; these factors and mechanisms are important when selecting suitable controlling methods for the BD, improving its suppression efficiency, and evaluating its recycling feasibility.

2. Experimental

2.1. Materials

2.1.1. Sample collection

As shown in Fig. 1, the BD sample researched in this study was collected from the Meishan iron mine, located in Nanjing, China. Before blasting, a plate with dimensions 60 cm × 80 cm was fixed 25–30 m from the blasting face using the method described by Fujiwara *et al.* [25]. 1.5 h after blasting, the BD sample was collected from the plate and immediately transported to the laboratory in a plastic pouch to prevent further contamination.
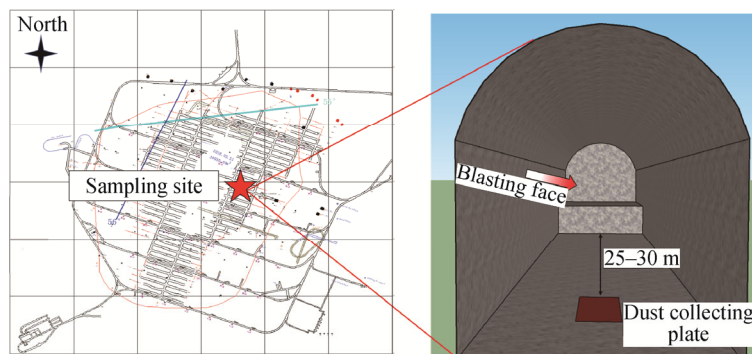

Fig. 1.   Maps showing the location of the sampling site (left) and a schematic of the sampling method (right).

2.1.2. Sample pretreatment

Unlike the studies conducted by Yang *et al.* [20] and Li

et al. [17], no crushing or grinding operation was performed for the original sample to ensure that the natural physico-

chemical properties of the sample remained unchanged. Only screening was used to remove large (≥ 74.16 μm) particles. Next, the screened sample was dried under high vacuum at 100°C for 2 h to remove its surface moisture and reduce its influence on the separation experiment [24]. Thereafter, the dried BD sample was slowly poured into a beaker containing deionized water (the surface tension of the water was 73.02 mN/m). Fig. 2 clearly shows that the sample was divided into two parts: UWBD that floated on the surface of the deionized water and WBD that sank [16]. These parts correspond to the hydrophobic and hydrophilic parts of the BD, respectively. After 2 min, the UWBD and WBD were extracted using a slide glass and then dried again at 100°C for 2 h [2]. The pretreatment of the sample was complete at this point.
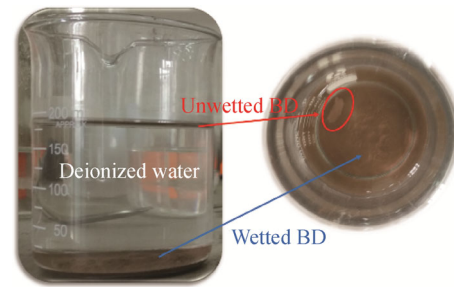

Fig. 2.   Unwetted and wetted BD in deionized water.

2.2. Experiments

To explore the key factors affecting the wettability of the BD, the physical and chemical properties of the UWBD and WBD were comprehensively characterized and compared with each other. The entire experimental process is shown in Fig. 3.
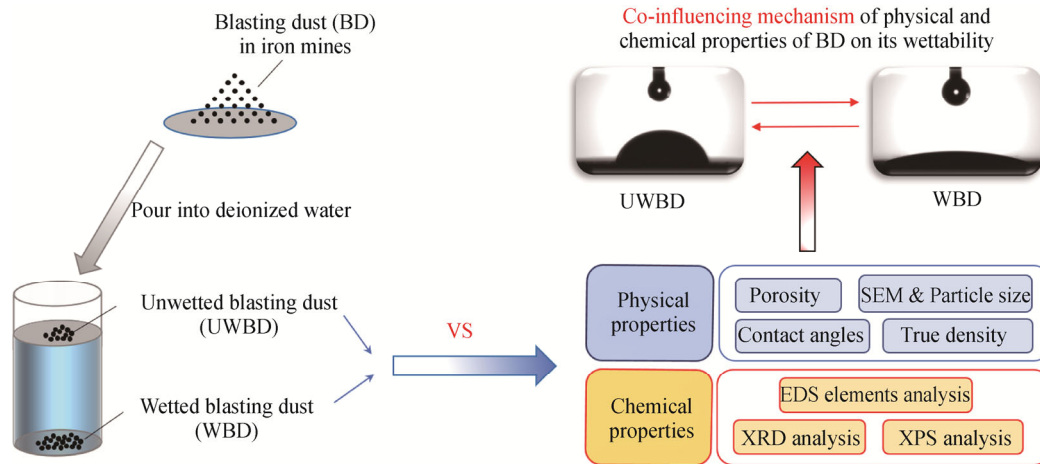

Fig. 3.   Characterized process of BD physicochemical properties used in the present work.

2.2.1. Characterization of physical properties

The dynamic contact angles (CAs) between the deionized water and the UWBD and WBD blocks (molded at 50 MPa) were measured on a Theta Lite TL101 apparatus (Finland). The data were recorded and analyzed using the OneAttension software provided by the instrument manufacturer. The PSDs of the UWBD and WBD were characterized using a laser particle size analyzer (LPSA) (Winner 2000, China) with anhydrous ethanol as the dispersion liquid [26]. Before the test, the bubbles in the liquid were crushed by ultrasonic waves generated by an ultrasonicator attached to the LPSA. The experiments are repeated three times, and the average value was analyzed. The micromorphology of the UWBD and WBD were observed using a scanning electron microscope (SU8000, Japan). Subsequently, the ImageJ software was used to measure the particle size from scanning electron microscope (SEM) images to verify the LPSA results. Among numerous methods for pore characterization,

low-pressure N_2 gas adsorption (LP-N_2GA) analysis has been verified to be an effective method to investigate the pore structure of a porous medium [27]. Therefore, the porosity parameters of the UWBD and WBD, including their pore size distributions, pore volume, pore area, and SSA, were analyzed via an LP-N_2GA experiment (3H-2000PS2, China) at liquid-nitrogen temperature (77 K at 101.3 kPa), which was conducted according to Chinese national standard GB/T 21650.3−2011.

The true density (TD) of particulates apparently affects their deposition characteristics in water by affecting their acceleration under gravity [16]. However, very few studies have considered this parameter. In the present study, the TDs of the UWBD and WBD were tested on the basis of Archimedes' principle using an automatic true density analyzer (3H-2000TD, China). As shown in Fig. 4, the steps and calculation procedures of samples are as follows:

First, X g of sample (with true volume V_X) was placed

into the sample cell (with volume V_{SC}); the remaining volume V_2 of the sample cell is expressed as

$$V_2 = V_{SC} - V_X \tag{1}$$

Then, valves 1, 3, and 4 are closed, and valve 2 was opened. Pressure P_1 was recorded until the pressure stabilized.

Next, valve 2 was closed, and valve 1 was opened. The reference cavity (with volume V_1) was inflated to a specified pressure, then valve 1 was closed, and pressure P_2 was recorded. The molar amount of gas n_1 in the system (the sum of the reference cavity and the sample cell) is expressed according to Bohr's law as

$$n_1 RT = P_1 V_2 + P_2 V_1 \tag{2}$$

Finally, valve 2 was opened, and pressure P_3 was recorded until it stabilized. The molar amount of gas n_2 in the system was expressed as

$$n_2 RT = P_3(V_1 + V_2) \tag{3}$$

Eq. (4) can be obtained by applying the condition $n_1 = n_2$:

$$V_2 = \frac{(P_2 - P_3)V_1}{P_3 - P_1} \tag{4}$$

Hence, V_X can be obtained by Eqs. (1) and (4), as expressed in Eq. (5):

$$V_X = V_{SC} - \frac{(P_2 - P_3)V_1}{P_3 - P_1} \tag{5}$$

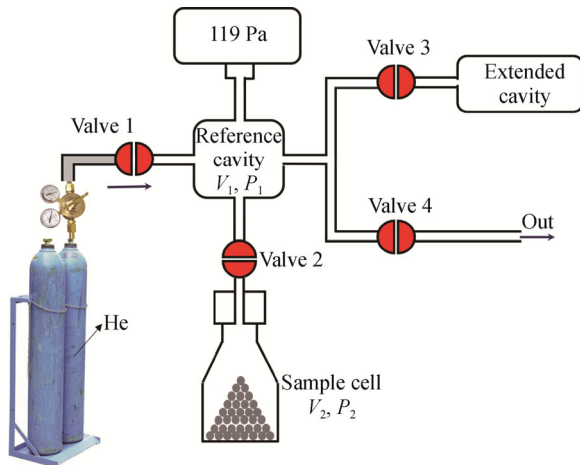Therefore, the TD (g/cm^3) of the testing sample is the ratio of X to V_X.

Fig. 4.   Diagram of the true density testing mechanism.

2.2.2. Characterization of chemical properties

The elements, mineral composition, and surface carbon compounds of the UWBD and WBD were characterized using energy dispersive X-ray spectrometry (EDS), X-ray powder diffraction (XRD), and X-ray photoelectron spectroscopy (XPS), respectively. The elemental analysis of the UWBD and WBD with different particle sizes was performed using an EDS equipped on SU8000 in "spot mode" and "area mode," and the relative contents of each element were further analyzed via the intensity of the corresponding peak. The XRD patterns of the UWBD and WBD were obtained using an Ultima IV (Rigaku, Japan) operating at 40 kV and 40 mA with a Ni-filtered Cu Kα radiation source with a wavelength of 1.5406 nm. Diffractograms were recorded at diffraction angles from 5° to 100° at an angular speed of 2°/min. Further analysis was performed used the International Centre for Diffraction Data (ICDD) database and the MDI Jade 6.1 software. In addition, the adiabatic method was used to quantify the relative contents of each component in the test sample, and the weight fraction of component j was quantified, as expressed in Eq. (6):

$$w_j = \frac{I_j}{K_i^j \sum_{i=1}^{N} \frac{I_j}{K_i^j}} \tag{6}$$

where w_j is the weight fraction of compound j, I_j is the diffraction intensity of component j, which can be replaced by the area of the strongest peak, K is the parameter of each component, which can be obtained from the PDF cards in the ICDD database, and N is the number of compounds in the test sample.

The carbon compounds on the surface of the UWBD and WBD were detected using an AXIS ULTRA spectrometer (Kratos, Japan) equipped with an Al Kα radiation source. The detection area was 700 μm × 300 μm. The binding energy of C 1s was corrected to 284.8 eV, and the energy spectrum of C 1s was used for hybrid fitting at 20% of Gauss–Lorentz function using the XPSPEAK 4.1 software. Moreover, the relative contents of each group were obtained by calculating the relative area ratio of the corresponding peak, as expressed in Eq. (7):

$$n_j = \frac{S_j}{\sum_{i=1}^{N} S_i} \tag{7}$$

where n_j is the relative contents of group j, S_j is the fitting peak area of group j, and N is the number of groups for C element.

3. Results and discussion

To verify the difference between the hydrophilicity of the UWBD and WBD, the dynamic CAs were tested for 2 s. As shown in Fig. 5, at 0 s, the CAs of the UWBD and WBD are 78.6° and 15.3°, respectively. Although the CAs of the UWBD and WBD decrease with time, the CA of the UWBD is greater than that of the WBD by approximately

15° at 0.4 to 2.0 s. Therefore, the hydrophobicity of the UWBD is stronger than that of the WBD, which introduces the possibility of exploring the effect of influencing factors on the hydrophilicity of the BD.
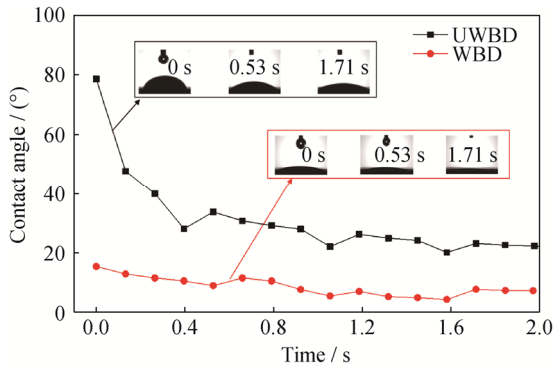

Fig. 5.   Dynamic contact angles and its varied curve of UWBD and WBD samples.

3.1. Differences in physical properties of UWBD and WBD

3.1.1. Differences in micromorphologies and particle sizes of UWBD and WBD

The particle size of dust is widely acknowledged to strongly affect its deposition properties in human airways. Generally, particulates with a particle size smaller than 10

μm can enter the human respiratory system; in particular, particles with diameters less than 1 μm can deposit in the alveolar region [28]. SEM is one of the most commonly used methods to observe the micromorphology and particle size of dust particles. The SEM images of the UWBD and WBD, shown in Fig. 6, are enlarged by 1000× and 800×, respectively. The large particles (particle size (PS) ≥ 10 μm), medium particles (10 μm > PS ≥ 1 μm), and nanoparticles (PS < 1 μm) are clearly observed in the UWBD image. The majority of the particles are medium particles; furthermore, most of them are irregular spheres with high surface roughness. Compared with the UWBD particles, most of the WBD particles are prismatic and are components of larger particles; that is, most of the WBD particles cannot be inhaled by humans. Thus, compared with the WBD, the UWBD not only exhibits greater hydrophobicity but also can be inhaled more easily, which poses a greater hazard to human health.

The specific PSDs of the UWBD and WBD evaluated using an LPSA are shown in Fig. 7; these PSDs are in good agreement with the particle sizes observed in the SEM images. The majority of particles of the UWBD and the WBD fall within the 1–10 μm range and in the larger than 10 μm range because, according to Kollipara *et al.* [16], heavier particles easily settle in water as a consequence of their high acceleration under gravity.
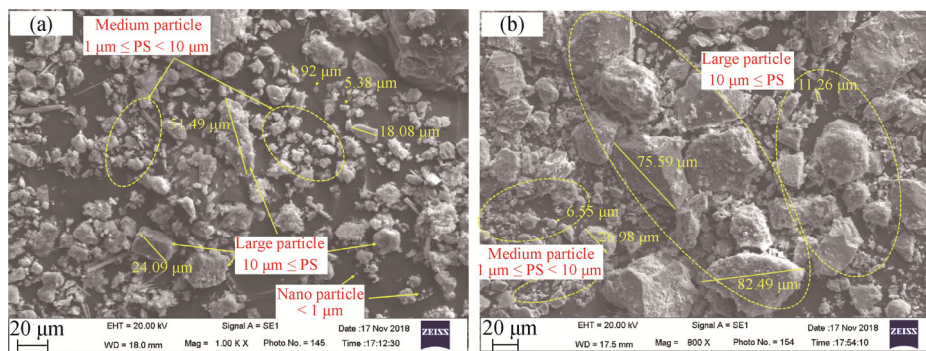

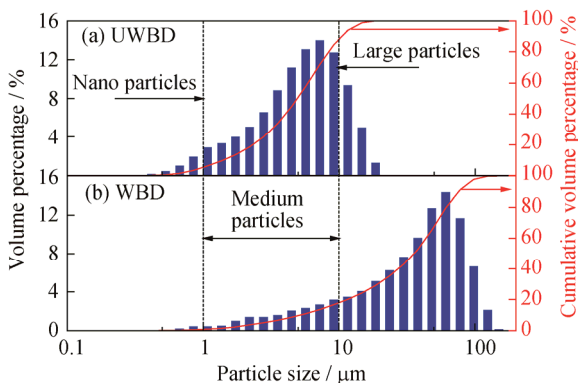**Fig. 6.   SEM images of (a) UWBD and (b) WBD samples (PS = particle size).**

Fig. 7.   Particle size distributions of (a) UWBD and (b) WBD samples.

Medium particles also occur in the WBD, as shown in Fig. 7 and Table 1. The d10, the particle size corresponding to 10vol% of the cumulative volume, of the WBD is 5.16 μm, which indicates that particle size is not the only factor affecting the wettability of the BD. Therefore, it is necessary to explore other factors that can influence the wettability of the BD by studying its other physical and chemical parameters.

3.1.2. Differences in TD and pore parameters of UWBD and WBD

According to Archimedes' principle, the relationship between gravity and buoyancy of dust determines whether it

sinks in water. Therefore, density is an important parameter in measuring the hydrophilicity of dust by the sink test. In this study, the TDs of the UWBD and WBD were measured as shown in Table 1. The TD of the WBD is 0.832 g/cm^3 greater than that of the UWBD; that is, each unit volume (1 cm^3) of the WBD is 8.32 mN heavier than that of the UWBD, which may affect the wetting process of the BD in water (compared with the surface tension value of 73.02

mN/m of deionized water). In addition, the difference in the TDs indicates that the main components of the UWBD and WBD indeed differ, which underscores the need to explore the differences in the physical and chemical properties of the UWBD and WBD in greater detail. Therefore, the results suggest that the TD should be tested before the wettability of the dust is characterized, particularly for sink tests such as the Walker test [29].

Table 1. Physical parameters of UWBD and WBD samples

| Sample | Particle size / μm | | | TD / (g·cm^{-3}) | SSA | | Pore volume | | | Pore size | | BJH cumulative pore area^e / (m^2·g^{-1}) |
	*d*10	*d*50	*d*90		BET SSA^a / (m^2·g^{-1})	Langmuir SSA / (m^2·g^{-1})	D–R micropore / (cm^3·g^{-1})	BJH mesopore^b / (cm^3·g^{-1})	Total volume^c / (cm^3·g^{-1})	BET pore size / nm	BJH pore size^d / nm	
UWBD	1.41	4.91	10.5	2.849	5.92	9.86	0.0020	0.0337	0.0357	20.95	14.58	10.07
WBD	5.16	35.51	75.43	3.681	3.74	6.07	0.0013	0.0173	0.0186	16.79	10.71	6.06

Notes: ^{a}SSA was determined using the BET equation with $0.0400 \leq p/p_0 \leq 0.3200$, where p/p_0 is the ratio of equilibrium pressure (p) to saturated vapor pressure(p_0); ^{b}Pore diameter ranges from 2.0–200 nm; ^{c}Total volume = micropore volume + mesopore volume; ^{d}Average values of adsorption pore size and desorption pore size; ^{e}Average values of adsorption pore area and desorption pore area; BET—Brunauer–Emmett–Teller method; D–R—Dubinn–Radushkevich method; BJH—Barrett–Joyner–Halenda method.
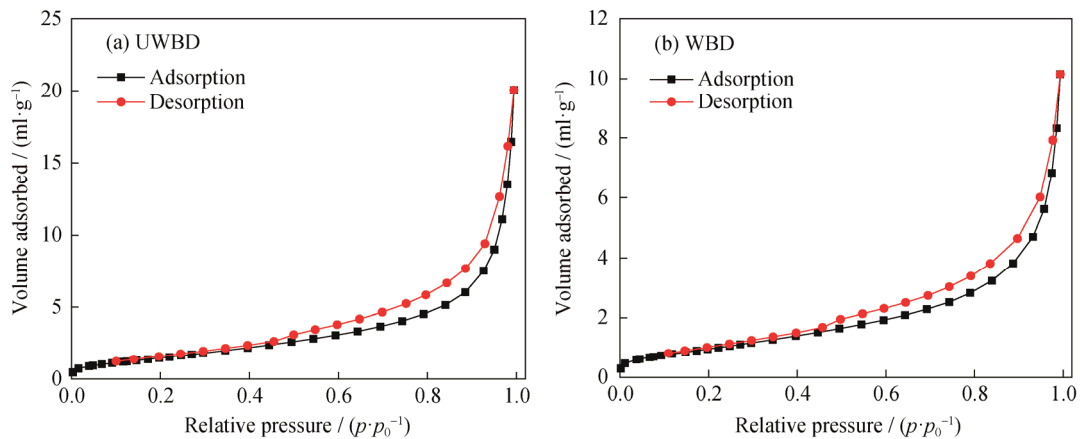

Fig. 8. Adsorption–desorption isotherms of the UWBD and WBD samples.

Pore properties of the UWBD and WBD were also determined via the LP-N$_2$GA experiment. Their type C adsorption–desorption isotherms [30] are shown in Fig. 8. It can be seen that the absorbed N$_2$ volume of the UWBD at the highest pressure is 20.06 cm^3/g, which is almost twice than that of the WBD (10.15 cm^3/g) and is also much higher than that of the respirable coal dust (varying in 10–14 cm^3/g) as reported by Yang *et al.* [20]. This demonstrates that there exist abundant pore structures in the UWBD, which may be related to the action of huge detonation waves. In addition, the SSA, pore volume, pore size, and cumulative pore area are computed using the equations of Brunauer–Emmett–Teller (BET), Langmuir, Dubinn–Radushkevich (D–R), and Barrett–Joyner–Halenda (BJH) methods, respectively, as presented in Table 1. The data show that the BET SSA and

Langmuir SSA of the UWBD are 1.58 and 1.62 times that of the WBD, respectively; and the mesopore volume of the UWBD is also much larger than that of the WBD, resulting in the total volume of the UWBD being 1.92 times that of the WBD. Moreover, it is noted that the BET and BJH pore sizes of the UWBD are larger than that of the WBD although the particle size of the UWBD is less than that of the WBD. Lastly, the BJH cumulative pore area of the UWBD is also 4.01 m^2/g larger than that of the WBD, suggesting that there are more pore structures in the UWBD compared to the WBD, which not only increases the surface area of dust, but also provides a wide range of places for air adhesion on its surface, which significantly weakens the wettability of the UWBD [17,20].

In addition, the pore size distribution was obtained using

the DFT (density functional theory) model, which is a much more accurate approach for pore size analysis and bridging the gap between the molecular level and macroscopic approaches [21]. As shown in Fig. 9, a pair of similar unimodal curves is observed. The dominant size lies between 0.5 nm and 100 nm for the UWBD and WBD, with the major peak at approximately 1 nm, which is apparently smaller than that of respirable coal dust according to Li *et al.* [17] and Yang *et al.* [20]. This result again shows that the BD has a high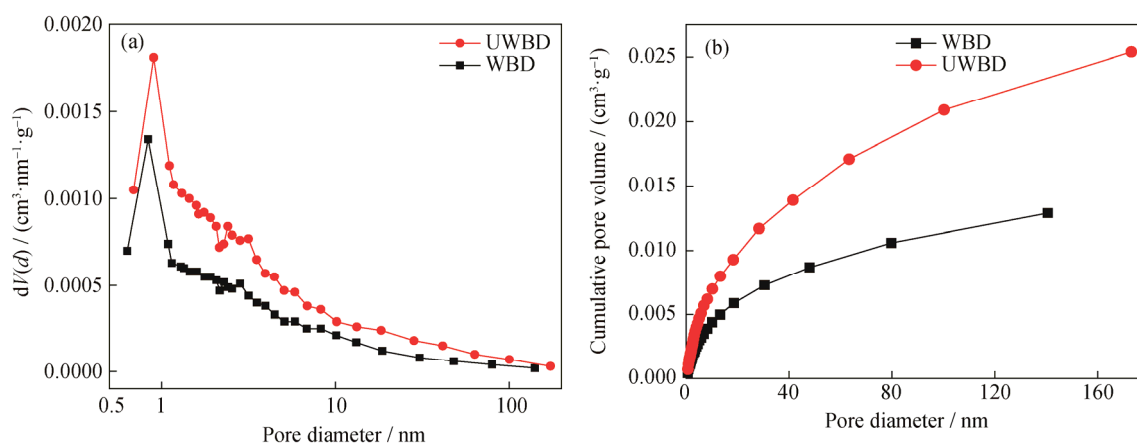er and more complex pore structure because the rock with high hardness is destroyed more thoroughly under the violent action of the detonation wave, whereas coal dust is formed by crushing, cutting, and friction. Furthermore, the differential volume of the UWBD is larger than that of the WBD in each description range, which verifies the pore volume results obtained using D–R and BJH methods, as shown in Table 1. Specifically, the rather developed pore structure in the UWBD is a key cause of its poor wettability because of the large amount of air adsorbed onto its surface.

Fig. 9.   Differential pore volume (a) and cumulative pore volume (b) of UWBD and WBD samples.

3.2. Differences in chemical properties of UWBD and WBD

As reported by Tian and Jiang [31], surface energy, which depends on the surface's chemical composition, is a key factor determining the wettability of solid materials. We therefore characterized the element, mineral composition, and surface compounds of the UWBD and WBD, as described in this section.

3.2.1. Element differences in UWBD and WBD

The elements and their relative contents of the UWBD and WBD with different particle sizes were measured using the "spot mode" for large particles (> 10 μm) and the "area mode" for small particles (< 10 μm), as shown in Fig. 10. C, O, Si, and Fe are the four elements in each image. Notably, the content of Fe is apparently less in the UWBD than in the WBD. The relative atomic mass of element Fe is higher than those of elements C, O, Si, Al, and Mg. Hence, the greater the content of element Fe the matter contains, the greater its density. This observation is in agreement with the TD test results presented in Section 3.1.2. Therefore, the TD of the UWBD is less than that of the WBD because its Fe content is lower. In combination with the results in Fig. 7, these results imply that the mineral with greater element Fe content is not likely to form small particles during the blasting process because of its corresponding mechanical properties such as hardness; on the contrary, fewer Fe-containing substances such as quartz and calcite, are more likely to form smaller particles. This inference was verified by characterizing the mineral compositions and contents of Fe in the UWBD and WBD.

3.2.2. Differences in mineral compositions of UWBD and WBD

Five mineral compositions are observed in each XRD pattern of the UWBD and WBD, as shown in Fig. 11. The UWBD contains dolomite [CaMg(CO$_3$)$_2$], whereas the WBD contains ankerite [Ca(Fe^{2+},Mg)(CO$_3$)$_2$]. The remaining four components are the same: siderite (FeCO$_3$), hematite (Fe$_2$O$_3$), quartz (SiO$_2$), and calcite (CaCO$_3$).

Furthermore, the relative contents of five components were calculated using Eq. (6). As shown in Table 2, the content of CaMg(CO$_3$)$_2$ in the UWBD was less than the content of Ca(Fe^{2+},Mg)(CO$_3$)$_2$ in the WBD, whereas the sum of the relative contents of FeCO$_3$ and Fe$_2$O$_3$ in the UWBD and WBD were similar (39.9wt% and 40.0wt%, respectively). This result agrees well with that of the EDS test, which showed that the WBD contains more Fe than the

UWBD. Furthermore, the sum of the relative contents of CaCO$_3$ and SiO$_2$ (which do not contain Fe) in the UWBD was 49.3wt%, which is much higher than that in the WBD (29.3wt%), which verifies the inference from Section 3.2.1. The five minerals present in the UWBD and WBD are hy-

drophilic substances because of their high surface energy caused by the high polarity [31]. Therefore, the mineral composition of the BD does not directly affect its wetting properties; however, it indirectly affects the deposition cha-racteristics of the BD in water by influencing its TD.
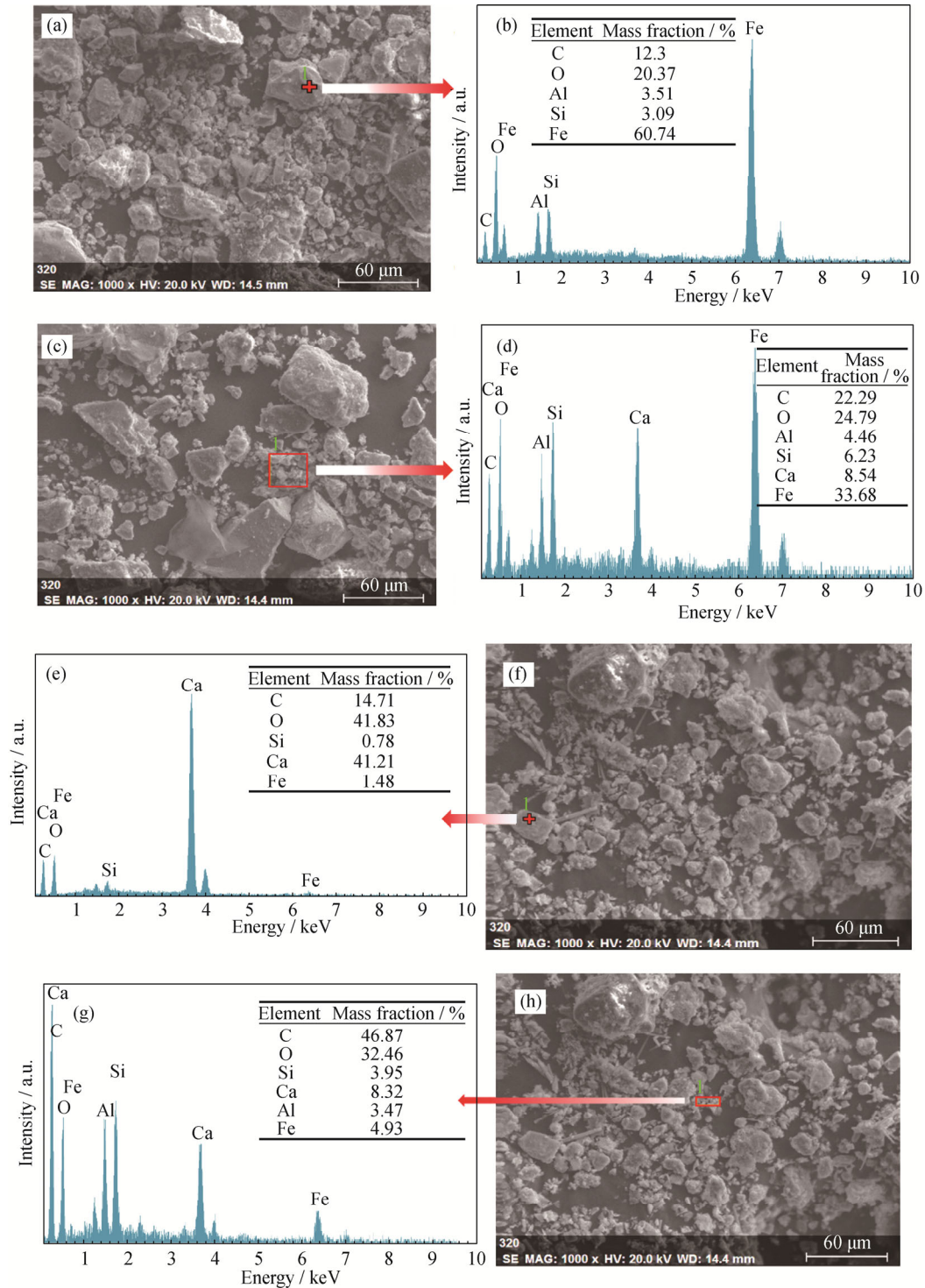

Fig. 10.   **Elements and SEM images of WBD and UWBD samples: (a, b) large particles of WBD; (c, d) small particles of WBD; (e, f) large particles of the UWBD; (g, h) small particles of the UWBD.**
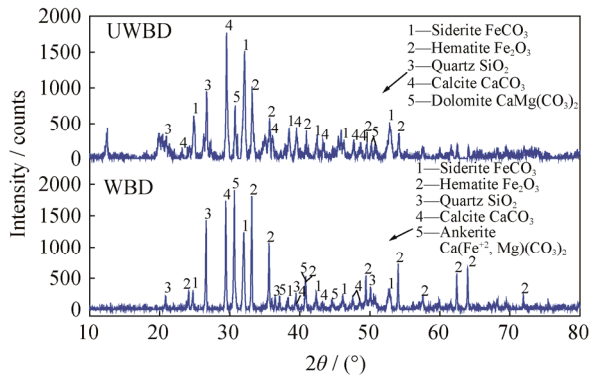
Fig. 11. XRD patterns of UWBD and WBD samples.

Table 2. Mass fraction of five mineral compositions in UWBD and WBD samples

Mineral compositions	Mass fraction / %	
	UWBD	WBD
$CaCO_3$	25.3	19.2
Fe_2O_3	14.4	19.6
$FeCO_3$	25.5	20.4
SiO_2	24.0	10.1
$CaMg(CO_3)_2$	10.8	—
$Ca(Fe^{+2}, Mg)(CO_3)_2$	—	30.7

Lastly, the content of quartz in the UWBD (24.0wt%) is higher than that in the WBD (10.1wt%), indicating that inhaled UWBD is more harmful to the human body than inhaled WBD because of its smaller particle size and higher quartz content (notably, quartz is the primary cause of silicosis). Therefore, effective control measures are needed for the UWBD after blasting in an iron mine.

3.2.3. Differences in surface compounds of UWBD and WBD

The surface chemical compounds of dust, particularly the organic matter, are widely accepted as strongly affecting its wettability [12,23−24]. Furthermore, organic carbon is the most representative organic matter in natural ores, formed by the deposition of decayed trees, leaves, and plants on the surface of ore. Although no obvious peaks of organic matter were observed in the XRD pattern, their presence in trace quantities is not ruled out. Therefore, we conducted XPS experiments to determine the organic carbon on the surface of the UWBD and WBD. As shown in Fig. 12, the C 1s spectrogram was divided into three peaks with different energy intensities using the peak-split and fitting process. The peaks at 285.1 eV correspond to C–C/C–H groups, those at 286.7 eV and 287.3 eV correspond to C–O/C=O groups, and that at 289.7 eV corresponds to MCO_3 groups [20,24].
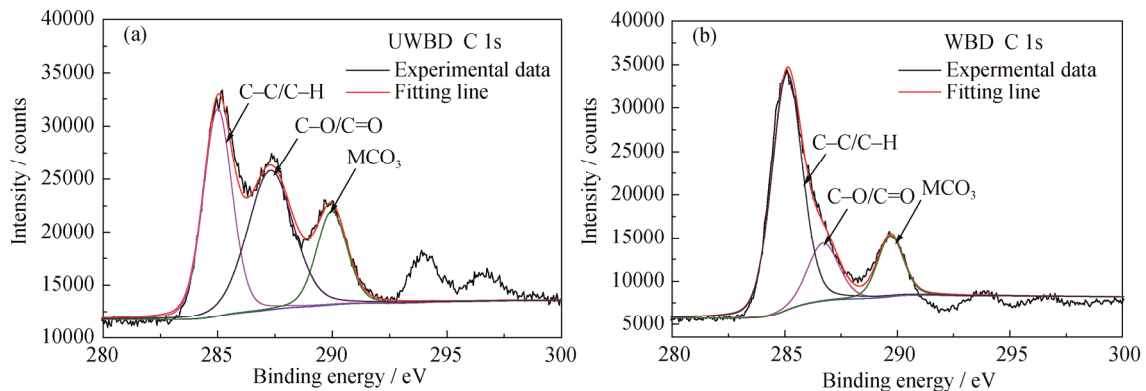

Fig. 12. XPS C 1s spectrum and its peak fitting lines of (a) UWBD and (b) WBD samples.

The relative contents of each group were calculated by considering their relative component (RC) peak areas [24]; the results are shown in Table 3. In particular, the sum of the RC peak areas of hydrophilic groups C–O/C=O and MCO_3 (63.97%) in the UWBD is much larger than that in the WBD (31.70%). This difference indicates that, although the surface organic composition plays a dominant role in the wettability of the coal dust [23−24], it does not affect the UWBD. This observation can be explained as follows. First, the overall content of the surface hydrophobic organic matter was relatively low because no obvious organic matter was observed in the XRD pattern. Second, the unique phys-

ical structure of the UWBD—that is, the complex pore structure and smaller TD—may have caused this effect. The special physical properties of the UWBD not only reduce its gravity but also form a complete air film on its surface, which is an essential reason for its greater hydrophobicity.

3.3. Influence of physicochemical properties of BD on its hydrophilicity

According to the aforementioned experimental results and the results of some previous studies [16,21,23,26,31−34], the co-influencing processes of physical and chemical properties of dust on its wettability are proposed (Fig. 13). Ele-

ven influencing processes are summarized as follows: (1) Porosity is an important physical property of dust, and high porosity can provide numerous sites for the adsorption of air, leading to the formation of an air film on the dust surface [21], thereby weakening its wettability. (2) The particle size of dust is another physical factor that directly affects the wetting characteristic of dust: the smaller the particle size, the larger the SSA, the higher the surface energy, and the easier the adsorption of air [17,20,31]. (3) In general, all minerals are hydrophilic in nature because of their high polarity induced by the coordinative unsaturation of the metal elements [31]. Hence, the more the minerals present in the dust, the stronger its hydrophilicity. (4) The aliphatic hydrocarbon group (C–C/C–H) of organic matter on the dust surface is hydrophobic in nature [23–24]. Thus, its content is negatively correlated with the hydrophilicity of the dust. (5) The formation mechanism of dust due to forces such as crushing, cutting, friction, and detonation wave also affect its porosity.

(6) The formation mechanism of dust affects its particle size because of the different destructive powers of these forces. The stronger the destructive power, the smaller the particle size and the greater the porosity. (7) Under the action of the same force, rock with different mechanical properties, such as different hardness and elasticity, is destroyed to different extents; the resulting dust then has different porosities. (8) For the same reason given in (7), dust can be composed of different particle sizes. (9) The mechanical property and (10) TD of rock are determined by the type of mineral. (11) Although the TD does not directly affect the wettability of the dust, it can influence the velocity of dust deposition in water. Therefore, to make the research data comparable, the TD of the dust should be determined first when using the sink test to study its wettability. As previously mentioned, the five physical and two chemical properties of the dust are co-related through eleven relations, which co-affect the wettability of the dust.

Table 3.   Peak positions and RC peak areas in C 1s spectrum

Sample	C–C/C–H[a]		C–O/C=O[b]		MCO₃[c]	
	Peak position / eV	RC peak area / %	Peak position / eV	RC peak area / %	Peak position / eV	RC peak area / %
UWBD	285.1	45.03	287.3	31.13	289.7	23.84
WBD	285.1	68.30	286.7	17.00	289.7	14.70

Notes: [a]Belongs to hydrophobic group; [b,c]Belong to hydrophilic group [20,24].
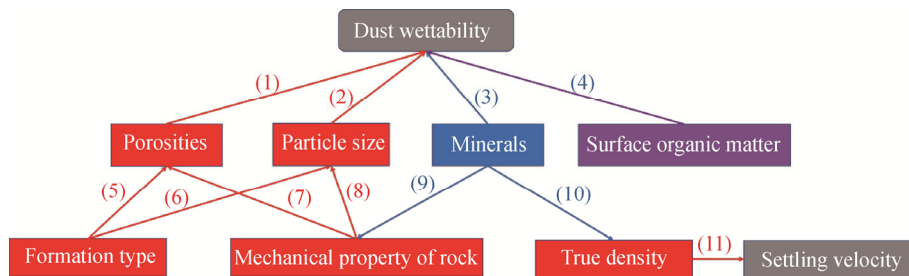

Fig. 13.   Influence of the physicochemical properties of dust on its wettability.

4. Conclusions

The BD of iron mines was divided into two parts—UWBD and WBD—using deionized water. The chemical and physical characteristics of the UWBD and WBD were comprehensively analyzed and compared with each other to explore the key factors affecting their wettability. The following conclusions were drawn from this study:

(1) Particle size and pore parameters are two key factors affecting the hydrophobicity of the BD: the smaller the particle size and the more developed the pore structure, the stronger the hydrophobicity of the BD.

(2) The mineral composition of the BD does not directly affect its wetting properties; however, it indirectly affects the deposition characteristics of the BD in water by influencing its TD. The TD of the UWBD and WBD was 2.849 g/cm^3 and 3.681 g/cm^3, respectively.

(3) Unlike coal dust, the surface organic composition of the BD does not affect its wettability, and the peak area of C–C/C–H hydrophobic groups in the UWBD (45.03%) is smaller than that in the WBD (68.30%).

(4) The wettability of the BD is co-affected by seven physicochemical factors—porosity, particle size, mineral contents, surface organic matter, formation type, mechanical property of the parent rock, and TD—and these factors influence each other through 11 processes.

Acknowledgements

References

[1] M. Akbari, G. Lashkaripour, A.Y. Bafghi, and M. Ghafoori, Blastability evaluation for rock mass fragmentation in Iran central iron ore mines, *Int. J. Min. Sci. Technol.*, 25(2015), No. 1, p. 59.

[2] J.G. Liu, L.Z. Jin, J.Y. Wang, S.N. Ou, J.Z. Guo, and T.Y. Wang, Micromorphology and physicochemical properties of hydrophobic blasting dust in iron mines, *Int. J. Miner. Metall. Mater.*, 26(2019), No. 6, p. 665.

[3] J. Csavina, J. Field, M.P. Taylor, S. Gao, A. Landázuri, E.A. Betterton, and A.E. Sáez, A review on the importance of metals and metalloids in atmospheric dust and aerosol from mining operations, *Sci. Total Environ.*, 433(2012), p. 58.

[4] B. Wang, C. Wu, L.G. Kang, G. Reniers, and L. Huang, Work safety in China's thirteenth five-year plan period (2016–2020): Current status, new challenges and future tasks, *Saf. Sci.*, 104(2018), p. 164.

[5] P. Gonzales, O. Felix, C. Alexander, E. Lutz, W. Ela, and A.E. Sáez, Laboratory dust generation and size-dependent characterization of metal and metalloid-contaminated mine tailings deposits, *J. Hazard. Mater.*, 280(2014), p. 619.

[6] Y.S. Sun, Y.X. Han, Y.F. Li, and Y.J. Li, Formation and characterization of metallic iron grains in coal-based reduction of oolitic iron ore, *Int. J. Miner. Metall. Mater.*, 24(2017), No. 2, p. 123.

[7] G. Zhou, B. Feng, W.J. Yin, and J.Y. Wang, Numerical simulations on airflow-dust diffusion rules with the use of coal cutter dust removal fans and related engineering applications in a fully-mechanized coal mining face, *Powder Technol.*, 339(2018), p. 354.

[8] G. Xu, K.D. Luxbacher, S. Ragab, J.L. Xu, and X.H. Ding, Computational fluid dynamics applied to mining engineering: A review, *Int. J. Min. Reclam. Environ.*, 31(2017), No. 4, p. 251.

[9] M.P. Taylor, S.A. Mould, L.J. Kristensen, and M. Rouillon, Environmental arsenic, cadmium and lead dust emissions from metal mine operations: Implications for environmental management, monitoring and human health, *Environ. Res.*, 135(2014), p. 296.

[10] S.B. Yang, W. Nie, S.S. Lv, Z.Q. Liu, H. Peng, X. Ma, P. Cai, and C.W. Xu, Effects of spraying pressure and installation angle of nozzles on atomization characteristics of external spraying system at a fully-mechanized mining face, *Powder Technol.*, 343(2019), p. 754.

[11] Z.L. Xi, M.M. Jiang, J.J. Yang, and X. Tu, Experimental study on advantages of foam–sol in coal dust control, *Process Saf. Environ. Prot.*, 92(2014), No. 6, p. 637.

[12] G. Xu, Y.P. Chen, J. Eksteen, and J.L. Xu, Surfactant-aided coal dust suppression: A review of evaluation methods and influencing factors, *Sci. Total Environ.*, 639(2018), p. 1060.

[13] D. Omane, W.V. Liu, and Y. Pourrahimian, Comparison of chemical suppressants under different atmospheric temperatures for the control of fugitive dust emission on mine haul's roads, *Atmos. Pollut. Res.*, 9(2018), No. 3, p. 561.

[14] Q. Zhou, B.T. Qin, J. Wang, H.T. Wang, and F. Wang, Effects of preparation parameters on the wetting features of surfactant-magnetized water for dust control in Luwa mine, China, *Powder Technol.*, 326(2018), p. 7.

[15] Y.P. Chen, G. Xu, J.X. Huang, J. Eksteen, X.F. Liu, and Z.D. Zhao, Characterization of coal particles wettability in surfactant solution by using four laboratory static tests, *Colloids Surf. A*, 567(2019), p. 304.

[16] V.K. Kollipara, Y.P. Chugh, and K. Mondal, Physical, mineralogical and wetting characteristics of dusts from Interior Basin coal mines, *Int. J. Coal Geol.*, 127(2014), p. 75.

[17] Q.Z. Li, B.Q. Lin, S. Zhao, and H.M. Dai, Surface physical properties and its effects on the wetting behaviors of respirable coal mine dust, *Powder Technol.*, 233(2013), p. 137.

[18] J.G.M.S. Machado, F.A. Brehm, C.A.M. Moraes, C.A. dos Santos, A.C.F. Vilela, and J.B.M. da Cunha, Chemical, physical, structural and morphological characterization of the electric arc furnace dust, *J. Hazard. Mater.* 136(2006), No. 3, p. 953.

[19] J.B. Zhu and H. Yan, Microstructure and properties of mullite-based porous ceramics produced from coal fly ash with added Al_2O_3, *Int. J. Miner. Metall. Mater.*, 24(2017), No. 3, p. 309.

[20] J. Yang, X.K. Wu, J.G. Gao, and G.P. Li, Surface characteristics and wetting mechanism of respirable coal dust, *Min. Sci. Technol.*, 20(2010), No. 3, p. 365.

[21] X.F. Liu, D.Z. Song, X.Q. He, Z.P. Wang, M.R. Zeng, and L.K. Wang, Quantitative analysis of coal nanopore characteristics using atomic force microscopy, *Powder Technol.*, 346(2019), p. 332.

[22] X.Q. He, X.F. Liu, D.Z. Song, and B.S. Nie, Effect of microstructure on electrical property of coal surface, *Appl. Surf. Sci.*, 483(2019), p. 713.

[23] C.H. Xu, D.M. Wang, H.T. Wang, H.H. Xin, L.Y. Ma, X.L. Zhu, Y. Zhang, and Q.G. Wang, Effects of chemical properties of coal dust on its wettability, *Powder Technol.*, 318(2017), p. 33.

[24] G. Zhou, C.C. Xu, W.M. Cheng, Q. Zhang, and W. Nie, Effects of oxygen element and oxygen-containing functional groups on surface wettability of coal dust with various metamorphic degrees based on XPS experiment, *J. Anal. Methods Chem.*, 2015, art. No. 467242.

[25] F.G. Fujiwara, D.R. Gómez, L. Dawidowski, P. Perelman, and A. Faggi, Metals associated with airborne particulate matter in road dust and tree bark collected in a megacity (Buenos Aires, Argentina), *Ecol. Indic.*, 11(2011), No. 2, p. 240.

[26] H.T. Wang, L. Zhang, D.M. Wang, and X.X. He, Experimental investigation on the wettability of respirable coal dust based on infrared spectroscopy and contact angle analysis, *Adv. Powder. Technol.*, 28(2017), No. 12, p. 3130.

[27] X.F. Liu, D.Z. Song, X.Q. He, B.S. Nie, and L.K. Wang, Insight into the macromolecular structural differences between hard coal and deformed soft coal, *Fuel*, 245(2019), p. 188.

[28] G. Oberdörster, E. Oberdörster, and J. Oberdörster, Nanotoxicology: An emerging discipline evolving from studies of ultrafine particles, *Environ. Health Perspect.*, 113(2005), No. 7, p. 823.

[29] P.L. Walker, E.E. Petersen, and C.C. Wright, Surface active agent phenomena in dust abatement, *Ind. Eng. Chem.*, 44(1952), No. 10, p. 2389.

[30] D.H. Everett and F.S. Stone, *The Structure and Properties of Porous Materials*, Butterworths, London, 1958.

[31] Y. Tian and L. Jiang, Wetting: Intrinsically robust hydrophobicity, *Nat. Mater.*, 12(2013), No. 4, p. 291.

[32] X.F. Liu, B.S. Nie, W.X. Wang, Z.P. Wang, and L. Zhang, The use of AFM in quantitative analysis of pore characteristics in coal and coal-bearing shale, *Mar. Pet. Geol.*, 105(2019), p. 331.

[33] X.F. Liu, D.Z. Song, X.Q. He, Z.P. Wang, M.R. Zeng, and L.K. Wang, Nanopore structure of deep-burial coals explored by AFM, *Fuel*, 246(2019), p. 9.

[34] T. Xu, X.J. Ning, G.W. Wang, W. Liang, J.L. Zhang, Y.J. Li, H.Y. Wang, and C.H. Jiang, Combustion characteristics and kinetic analysis of co-combustion between bag dust and pulverized coal, *Int. J. Miner. Metall. Mater.*, 25(2018), No. 12, p. 1412.